International Journal of Heat and Technology
Vol. 38, No. 2, June, 2020, pp. 525-532
Journal homepage: http://iieta.org/journals/ijht

Numerical Study of a Flow Through a Grid Placed in a Bunsen Burner

Mounir Benzitouni[1*], Zoubir Nemouchi[2], Mohamed Salah Boulahlib[1]

[1] Laboratoire Ingénierie des Transports et Environnement, Département Génie des Transports, Faculté des Sciences de la Technologie, Université Frères Mentouri Constantine 1, Constantine 25017, Algeria
[2] Laboratoire d'Energétique Appliquée et de Pollution, Département de Génie Mécanique, Faculté des Sciences de la Technologie, Université Frères Mentouri Constantine 1, Constantine 25017, Algeria

Corresponding Author Email: benzitouni.mounir@umc.edu.dz

https://doi.org/10.18280/ijht.380230

Received: 15 January 2019
Accepted: 20 March 2020

Keywords:
grid-generated turbulence, isothermal flow, turbulence intensity, multi-jet, perforated plate, numerical simulation

ABSTRACT

The present work is a numerical simulation of a turbulent isothermal flow through a grid placed in a tube, a simplified form of a Bunsen burner. The grid is a perforated plate with a blockage ratio of 54% and located 3D upstream of the exit of the tube of 25 mm in diameter (D). The holes have a diameter of 5.0 mm and the mesh size (M) is 7.0 mm. The flow is predicted using Large Eddy Simulation as implemented in the CFD code ANSYS FLUENT 14.5. The results obtained concerning lateral and streamwise distributions of mean velocities, velocity fluctuations and turbulent kinetic energy are presented in the forms of profiles and/or contours. The predictions are compared with experimental results available in the literature. They show that a nearly isotropic turbulence zone is reached at a streamwise position z/M=7.5 downstream of the plate and extends over a distance of about 2 M. They also show that the LES can reproduce the main characteristics of the flow velocity and intensity of the turbulence as obtained experimentally at the exit of the burner.

1. INTRODUCTION

The use of grids or perforated plates in the turbulent combustion field gives many advantages. For example, it reduces the turbulent flame stabilization problems (lift-off) associated with the use of lean premixed flame in gas turbines and furnaces [1]. In experimental laboratory research, grids are applied to generate different levels of turbulence intensity and control integral length scales to study flame-turbulence interactions [2, 3]. The production of turbulence intensity is achieved by placing a grid upstream of the burner exit [4]. In that situation the blockage ratio (defined as the ratio of the blocked area to the total surface), diameter of holes and mesh size play an important role in controlling the turbulence intensity level and the size of eddies [5]. For instance, Buschmann et al. [6] used different perforated plates of different diameter holes and blockage ratios to generate different flow turbulence intensities in the purpose to investigate the influence of the turbulence on the flame characteristics. It can be shown in their experiment that the turbulence is gaining in the intensity as the blockage ratio increases and the integral length scales also increase with the increase in the grid holes diameter. Gagnepain [7] and Gagnepain et al. [8] used two different perforated grids with two different blockage ratios (51% and 54%) to generate turbulence intensities of the order of 7.3% and 10.4% and integral length scales respectively of the order of 2.9 and 3.2 mm. Kalt et al. [9] were able to vary the turbulence intensity with only varying the position of a perforated grid placed upstream of the burner exit. Some recent works in the same research field have also been reported [10, 11]. However, this type of grid poses a serious problem when high turbulence intensity combined with good homogeneity and isotropy is needed. To overcome this situation, some classes of grids were proposed. Makita [12] developed an active grid which is composed of a bi-plane grid of round rods mounted with square wings oscillating by means of step motors each one driving a rod. He was then able to generate a high level of turbulence intensity of the order of 37% at a distance of X/M=10 (X is the streamwise coordinate and M is the mesh size) and 16% at a distance X/M=50 with nearly the same homogeneity and isotropy performance like that of a passive grid. An experimental study was conducted by Coppola et al. [5], to highlight the effects of two families of high-blockage perforated plates (with circular and non-circular openings), placed upstream of a profiled contraction on the turbulent flow field. For this purpose, they used hot-wire anemometry to measure mean axial velocity, turbulence intensity and turbulence length scales. The results obtained show that the non-circular central aperture plate represented the best compromise between the highest turbulence levels and excellent uniformity of mean velocity and turbulence intensity. Horender [13] conducted an experimental study for the measurements of streamwise velocity characteristics in a flow downstream of a perforated plate. The results show that the mean velocity decay on the centre line was much larger than that for a free jet but smaller than that for a confined jet. Flow visualizations have shown the existence of a highly turbulent reverse flow and suggest that the penetration of a turbulent fluid is larger than that of a laminar or low-turbulence fluid.

Another class of grids known as fractal grids is also proposed. The idea is based on the creation of different eddy sizes by just generating a fractal pattern on a passive grid. These types of grids exhibit more interesting turbulence behaviors than regular grids and may find better practical applications than that of active grids. Many experimental and

numerical works were carried out on the subject [3, 14-19] and showed that this type of grids generated higher turbulence intensity using a smaller blockage ratio than that of a regular grid with high blockage ratio and also created a broad range of multi-length scales depending on the geometrical grid characteristics. A comparison of the turbulence decay rate, performed by Krogstad and Davidson [16], between two fractal grids and a classical one showed that the fractal grid decay was close to that of the classical grid in the far field region. Fractal grids are gaining more and more interest in the turbulent premixed flame domain where it is possible to obtain, as mentioned above, a high level of turbulence intensity with only low blockage ratio and thus researchers were able to reproduce in laboratory experiments the industrial flow conditions as in gas turbine burners characterized by high turbulence intensities which is not possible to reproduce with classical perforated plates [3]. Another fact is that flame characteristics like Damköhler and Karlovitz numbers are influenced by turbulence velocity fluctuations and integral length scales of the flow. Soulopoulos et al. [20] compared the performance of fractal and classical grids, placed at the same position and given identical flow conditions in the burner. They showed that the turbulent flame velocity was higher than that obtained by a classical grid by more than 40% in average and the curvature and the flame brush were more pronounced.

Another promising configuration, known as mutli-scale grid, consisting of placing successive regular grids at the upstream of the burner exit to generate high intensity turbulence with different controlled length scales is used in that purpose. In the experiments reported by Mazellier et al. [14] and Fragner et al. [21], the multi-scale grid is composed of three perforated plates shifted in space such that the diameter of their holes and their blockage ratio increase with the downstream distance. Mazellier et al. [14] compared the performance of a multi-scale grid with a regular one (referred in their work as mono-scale grid and has geometrical characteristics as the last grid in the multi-scale grid device). They observed that the turbulence intensity in the homogeneous and isotropic region was larger in the multi-scale grid case than that in the mono-scale grid case. They also noted that isotropy was reached earlier than in the mono-scale grid case. In the experiment of Fragner et al. [21] the use of multi-scale grid under high pressure conditions was investigated. They found that this device induced a nearly homogeneous and isotropic turbulence in the potential core of an axisymmetric premixed burner and noted that the turbulent kinetic energy produced by the multi-scale grid was much larger than that produced downstream of the single-scale grid. More recently, Wang et al. [22] developed a multi-layer configuration comprised of perforated plates having different diameters of the holes. They could thus control the turbulence intensity and integral scale and investigate their effects on the flame performance.

Given the relative simplicity of the geometry of the classical plates placed in series compared to the fractal plates, the present work was motivated by the need to understand the flow through a conventional grid, a preliminary step to more complex studies on the turbulence of a multi-scale grid. The objective of the present study is to investigate numerically the three-dimensional flow through a perforated plate placed inside a tube. This configuration is similar to that used by Gagnepain [7]. The main aim is to evaluate the performance of a numerical tool in capturing mean and fluctuating parameters characterizing the dynamical behavior of the flow at the exit of a Bunsen burner.

2. COMPUTATIONAL DOMAIN AND NUMERICAL PARAMETERS

2.1 Geometrical configuration

The grid adopted in the present work is similar to those used in the experiment of Gagnepain [7]. This author used a perforated plate with a blockage ratio σ=54% placed at 50 mm (≈8 M) upstream of the burner exit to generate a fixed turbulence intensity of 10.4% at 5 mm downstream of the exit as shown in Figure 1.

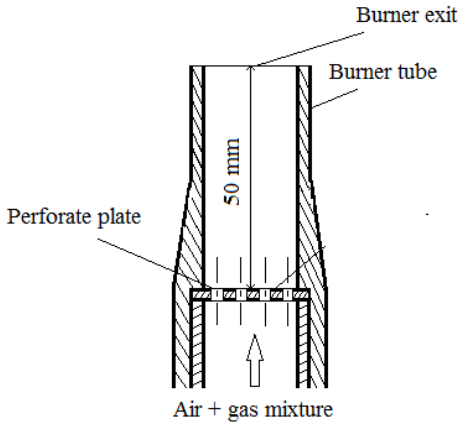

Figure 1. Schematic of a Bunsen burner with a perforated plate [7]

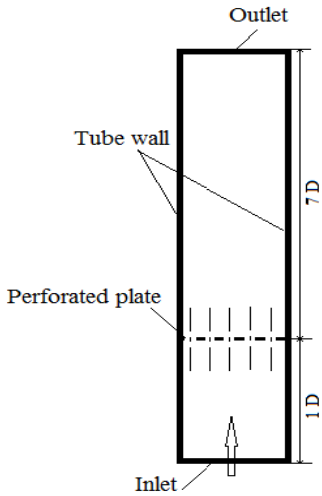

(a) Longitudinal section

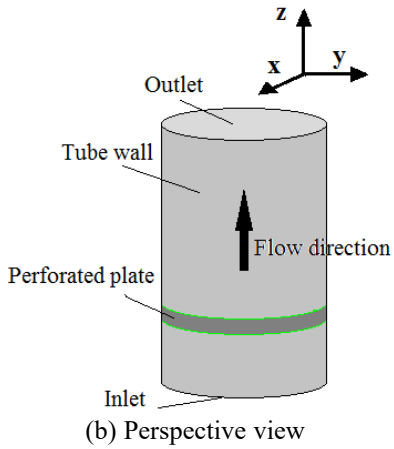

(b) Perspective view

Figure 2. Computational domain

The geometry is created and the numerical mesh is generated in the preprocessor GAMBIT. The burner is assumed to be a cylinder of diameter D=25 mm and of length L=8 D (Figure 2 (a)). The length of the domain exceeds that of the experiment, which is of length 2 D, in order to reduce to a minimum any upstream effect of the outlet boundary conditions on the turbulent flow behavior in the near field downstream of the perforated plate. The latter, of 3 mm thickness, is situated at a distance of one diameter from the domain inlet (Figure 2). The circular holes of the plate have a diameter d=5 mm and a pitch M=7 mm which correspond to a blockage ratio of 54%. The holes are placed in a hexagonal pattern as illustrated in Figure 3.

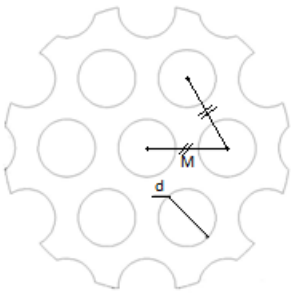

Figure 3. Perforated plate

2.2 Mesh generation and numerical approach

The mesh generated is composed of hexahedral volume elements. Three different meshes are used to test the sensitivity of the numerical solution: 2, 4 and 8 million nodes. Figure 4 depicts the effect of mesh resolution on the lateral distribution of the axial component of the mean velocity. The grid with 4 million nodes is used in this work as it gives results in accord with those obtained with the 8 million node grid.

A near wall (tube wall and perforated plate wall) refinement is accomplished to ensure that $y^+ \approx 1$. A finer mesh is also adopted in the near field (< 3 D), downstream of the plate to capture large velocity gradients. Outside this zone, the mesh is coarser in streamwise direction. The total number of cells composing the computational domain is 4 million.

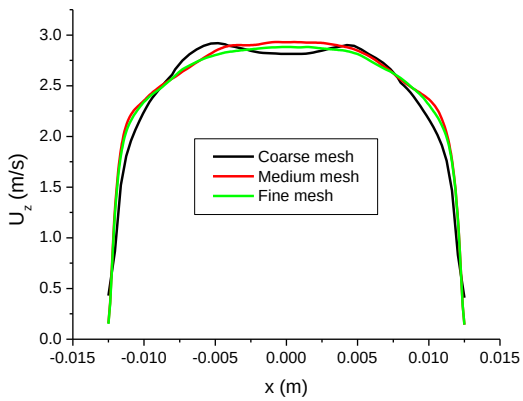

Figure 4. Effect of mesh resolution on the lateral distribution of the axial component of velocity at z=8 M

In order to validate the CFD code, Figure 5 compares present numerical predictions with measurements of the lateral variation of the axial component of velocity at the longitudinal position z=8 M. The top hat velocity profile at this position is relatively established in both cases.

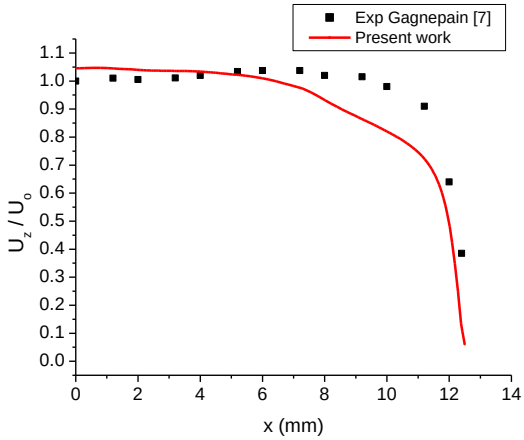

Figure 5. Lateral distribution of the axial component of velocity U_z normalized with the inlet velocity U_0

The 3D simulation is performed using the CFD code ANSYS FLUENT 14.5 based on the finite volume technique. The bounded central differencing scheme is used to discretize the convective term in the momentum equations. The flow is resolved with Large Eddy Simulation (LES) approach. The SIMPLE algorithm is used for the pressure – velocity coupling. The sub-grid scales are modeled with the Smagorinski-Lilly standard model. A second order implicit method is applied for the time discretization with a time step $\Delta t = 2 \times 10^{-05}$ s corresponding to 1/2500 of the mean flow residence time T defined as the ratio of the domain length L to the inlet velocity U_o. A first LES simulation is run until a flow development is reached. Computations were then performed for over 10 times T to obtain a statistically stable solution of the flow field.

2.3 Boundary conditions

A uniform velocity profile with no perturbation is imposed at the computational domain inlet. This is intended to eliminate any upstream turbulence contribution on the turbulence generated by the perforated plate. The inlet velocity is fixed at U_o=2.3 m/s. The fluid is air and is assumed incompressible and isothermal. A zero diffusion flux condition is imposed at the computational domain exit and no-slip condition is imposed at walls.

3. RESULTS

In the following, the streamwise axis z coincides with the tube axis and its origin is taken at the plate backward face position.

The Figure 6 shows the mean velocity magnitude contours in the xz plane at y=0. The flow passing through the plate behaves like a multi-jet case [13]. The deflection of jets is oriented towards the tube axis. It is more pronounced in the vicinity of the tube wall compared to that of the central jets. It is well known that jet spreading is accompanied with an entrainment of the surrounding air. In the present configuration, the entrainment causes a high relative suction between adjacent jets than that occurring between a jet and the tube wall immediately downstream of the plate. This observation is also reported by Tanaka [23] in the case of channel flow.

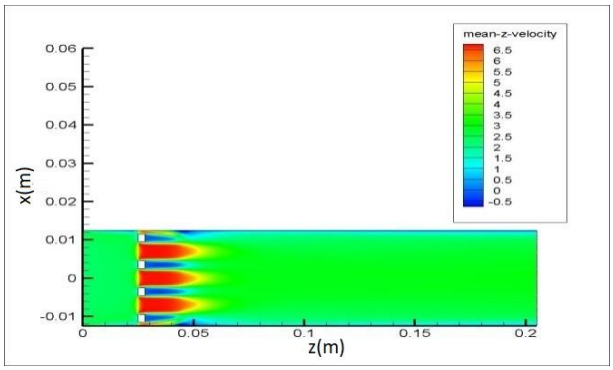

Figure 6. Contours of the mean velocity magnitude in the xz plane

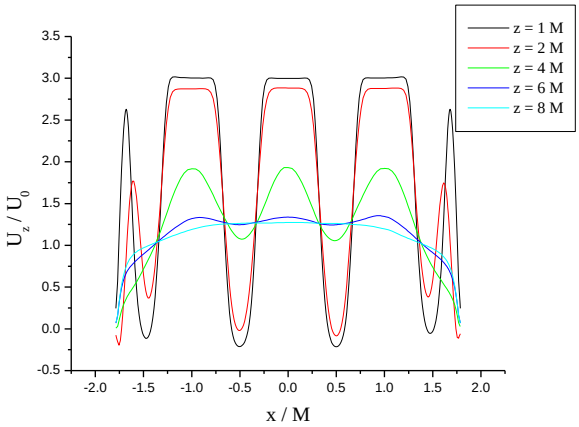

(a) Positions from z=1 M to 8 M

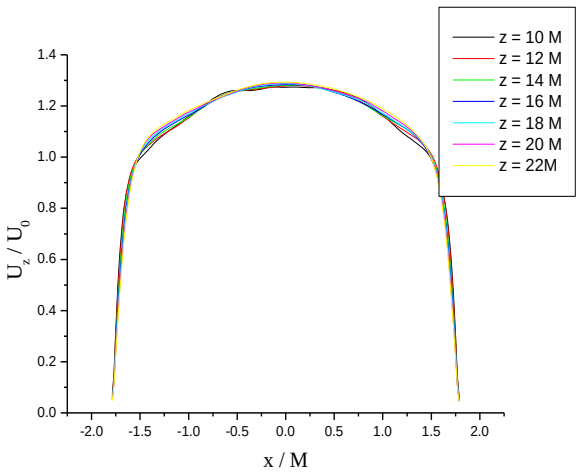

(b) Positions from z=10 M to 22 M

Figure 7. Lateral distributions of the normalized axial component of the mean velocity with the velocity inlet U_o in x direction at different positions downstream of the plate (positions progressing in the streamwise direction and are function of the mesh size M)

High velocity magnitudes are encountered in the near field region due to the acceleration of the flow imposed by the plate holes contractions. The lateral distribution in the x direction of non-dimensional velocity (defined as the ratio between the axial component of the mean velocity U_z and mean inlet velocity U_o) at different streamwise stations normalized with mesh size M downstream of the plate is illustrated in Figure 7. The mean velocity profiles take a top hat shape in the vicinity of the plate. Negative values are noted at the position 2 M, indicating flow reversal in those regions. At the position 6 M, the momentum has appreciably diffused in the lateral direction.

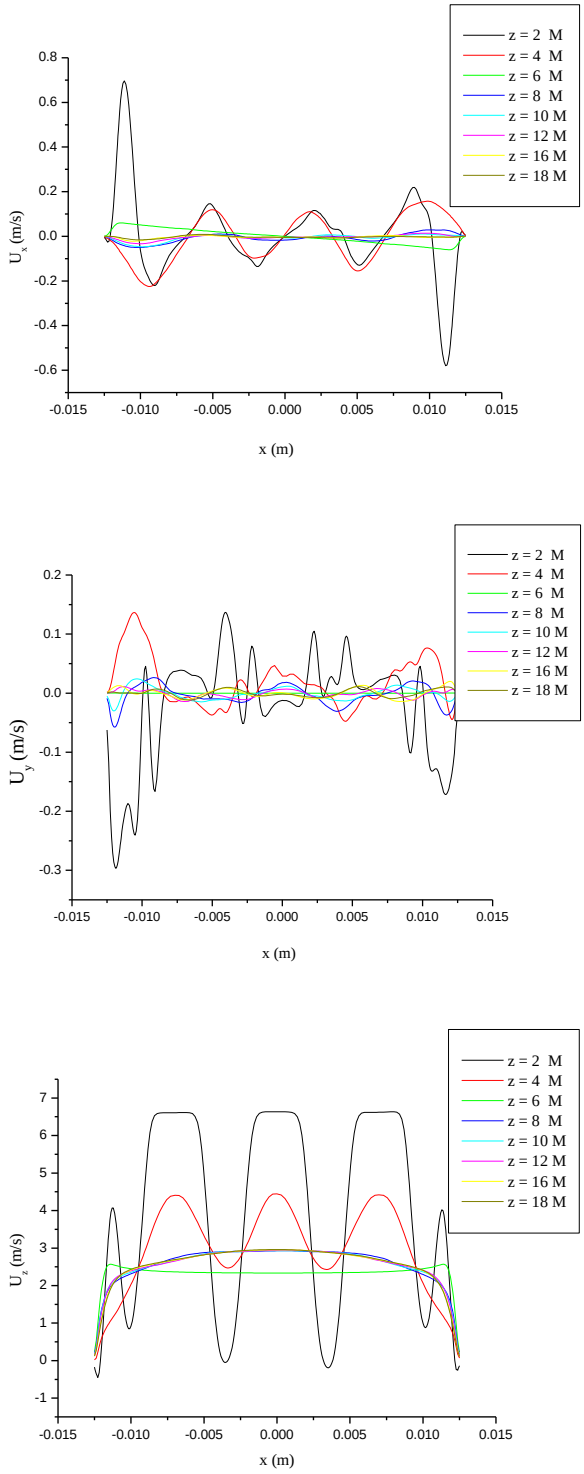

Figure 8. Lateral distribution of mean velocity components (U_x, U_y and U_z)

The maximum velocity is about three times the mean velocity U_o at the inlet. Individual jets are well identified in Figure 7 (a). Negative velocities are observed in the region just downstream of the plate indicating the presence of a recirculation flow. Maximum velocities decrease in

streamwise direction and jets merge together and disappear completely at a distance of about z=8 M from the plate with a velocity profile wider than that of an individual jet issuing from hole. The mean velocity profile then becomes more homogenous from the position z=8 M and farther downstream Figure 7 (b). The choice of the axial mean velocity U_z is motivated by the fact that the flow is dominated by this component as shown in Figure 8.

The streamwise variation, along the tube axis, of the turbulent energy k equal to 0.5 $\left(u_z^2 + u_x^2 + u_y^2\right)$ exhibits two main evolutions (Figure 9). A rapid production zone which lies between streamwise positions 0.5 and 4.57 M and a decay zone after that. It should be noted that the decrease is very rapid at first and becomes much slower further downstream. The contours in Figure 10 highlight clearly the zones of high turbulence production (in red) characterized by high velocity gradients.

The streamwise distribution, along the tube axis, of the turbulence intensity defined as the ratio of the root mean square (rms) of the axial velocity fluctuation u_z and the local axial mean velocity U_z is illustrated in Figure 11.

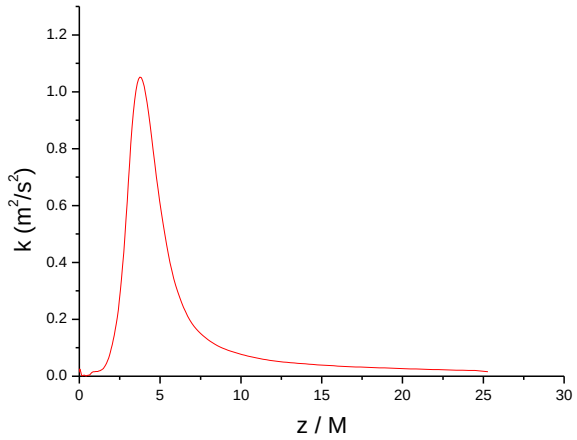

Figure 9. The streamwise distribution of the turbulent kinetic energy k versus the distance z normalized with M

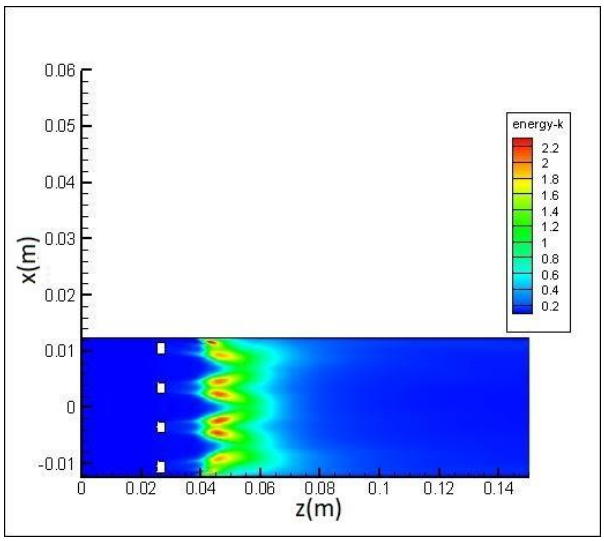

Figure 10. Contours of the turbulent kinetic energy k in the xz plane

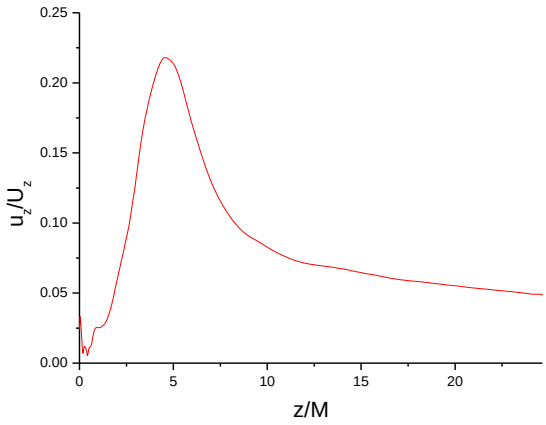

Figure 11. The axial distribution of the turbulence intensity u_z/U_z as a function of z normalized with the mesh size M

The intensity of turbulence is an essential data, which can give access to the power law correlations. In Figure 11, we observe a significant increase in u_z/U_z with the distance from the grid, up to a position z/M=5 corresponding to the end of the jet potential core, then the jet adopts a fast decay to z/M=10. Then we observe that it is gradually dissipated by viscous friction.

Figure 12 compares the predicted radial profile of the turbulence intensity (rms-value of the streamwise velocity fluctuation normalized by the local mean velocity) obtained in the present work with that measured by Gagnepain [7], downstream of the plate, at the position z=8 M. The agreement is fairly satisfactory in the core region from the tube axis up to a radius of 0.4 M. Beyond this radial position, the computed intensity deviates appreciably from the experimental data indicating an overestimation of the turbulent fluctuations in the simulation, in the annular zone away from the axis. The turbulence predicted by this simulation survives longer than that in the experiment. Another probable source of discrepancy is the fact that in the computational domain, the position z/M=8 M is inside the tube, whereas in the experiment, it is 5 mm downstream of the tube outlet.

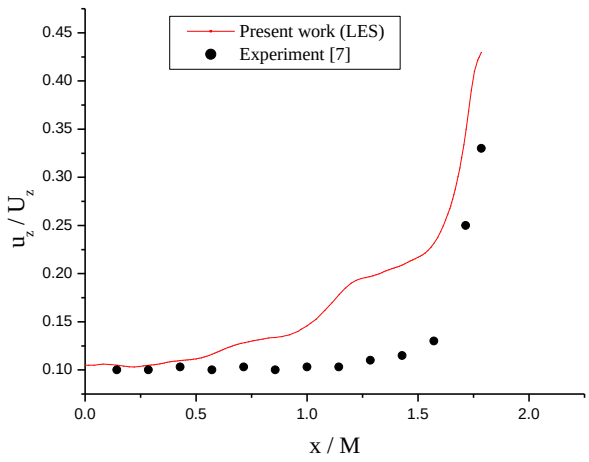

Figure 12. Radial distribution of the streamwise turbulent intensity at the position z=8 M

Figure 13 illustrates the streamwise evolution, along the tube axis, of the three velocity fluctuation components (rms values). The peak of the turbulent fluctuations is observed at a distance of 4.57 M from the plate. Then the rms values decrease to 0.15 m/s for u_z and 0.09 m/s for u_x and u_y at the end of the computational domain. The streamwise fluctuation is relatively more intense compared to the other two components. This may be due to the fact that the mixing layer at the periphery of the jet just downstream of the plate central hole produces a streamwise velocity fluctuation higher than the two cross-stream components. Such an anisotropic turbulence is convected downstream and part of it is diffused towards the tube axis. The cross-stream fluctuations u_x and u_y seem to evolve in a practically identical manner. To evaluate the isotropy, the ratio of the streamwise to the cross-stream velocity fluctuation u_z/u_y is considered as well as the ratio u_x/u_y. These parameters are similar to those investigated by Comte-Bellot and Corrsin [24]. It can be seen, in Figure 14, that the ratio of the lateral components u_x and u_y is of the order of 1 ($u_x/u_y \approx 1$) downstream of the plate. At all positions u_z is higher than u_x and u_y.

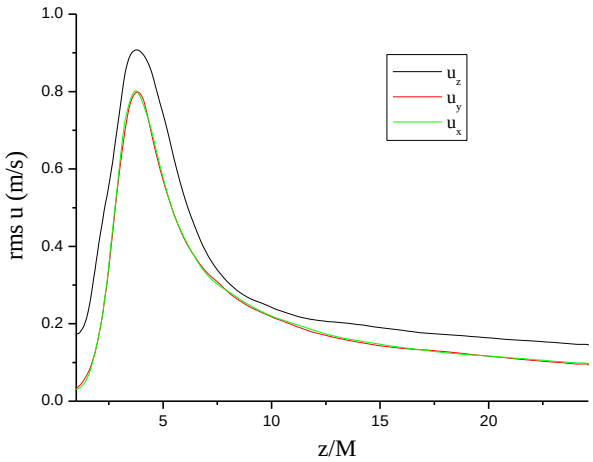

Figure 13. Variations of the rms values of the velocity fluctuation components along tube axis

There is a small region (7.5<z/M<9.5) where the streamwise fluctuation is somewhat close to the other components implying a fairly isotropic state of turbulence. Upstream of the position z/M=7.5, the streamwise fluctuation component is much more important than the other two. In fact, it may be a non-turbulent perturbation induced by the instability in the mixing layer surrounding the jet potential core. Downstream of the position z/M=11.5, the anisotropy grows up fairly rapidly and that is probably due to the streamwise-fluctuation-dominated turbulence generated in the boundary layer near the tube wall and diffused radially towards the axis. The ratio u_z/u_y increases from 1.1 to 1.4 in the streamwise direction.

Figure 15 exhibits contours of the filtered velocity magnitude in the xz plane. The flow remains quite organized up to the position z=1 M downstream of the plate, whether in the core of the jets or in the viscous flow in the mixing layers around the jets and in the recirculating zones behind the plate wall. Distortions of the jets are observed beyond this position. The jet potential cores disappear completely at about z=1.5 M and the flow structures break down and attain a fully turbulent regime. The contours of the subgrid turbulent viscosity in Figure 16 indicate clearly the frontiers between turbulent and non-turbulent zones in the flow. They also show the strong inhomogeneity characterizing the turbulent fluctuations.

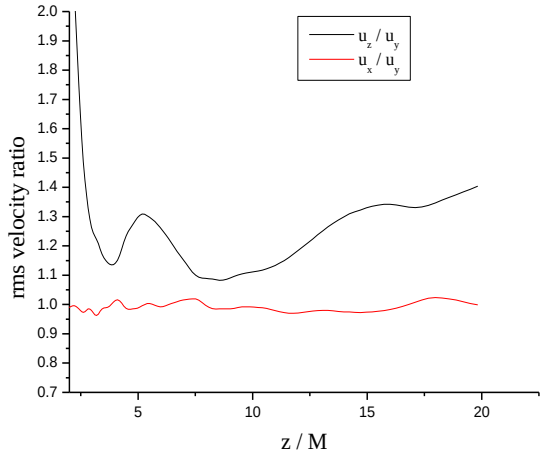

Figure 14. Variations of rms velocity ratios along tube axis, for isotropic evaluation

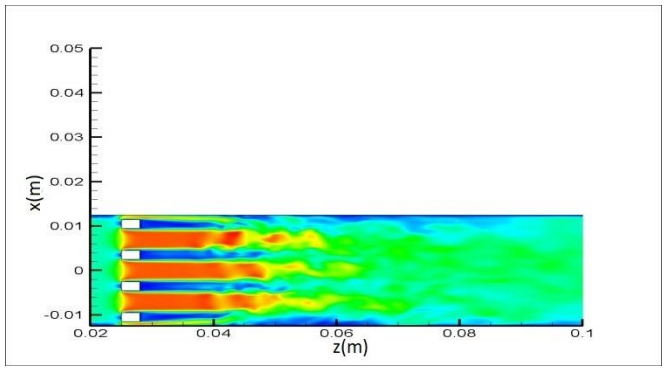

Figure 15. Filtered contours of the velocity magnitude in xz plane

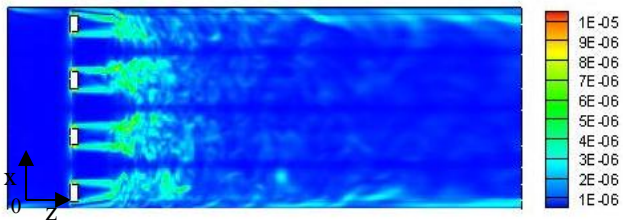

Figure 16. Contours of the subgrid turbulent viscosity

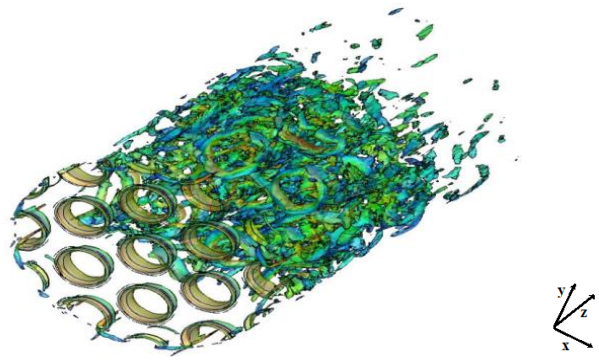

Figure 17. Isosurface of Q-factor

Figure 17 depicts an isosurface of the Q-factor ($Q = 0.5\ (\omega^2 - S^2)$), as defined in Hunt et al. [25]. It allows the visualization of the growth and advancement of the vortical structures downstream of the perforated plate. ω is the vorticity magnitude and S is the strain rate. Toroidal vortices are well identified at a distance comprised between 1 M and 2 M downstream of the plate. Such coherent structures quickly breakdown to form tube structures which in turn disintegrate into non-identifiable structures mostly of a little volume. The ring structures evolution could explain the jets disturbances observed and interaction of jets occurs when these structures stretch.

4. CONCLUSIONS

A numerical study is conducted to characterize the flow behind a grid confined in a tube using the LES approach. Special attention is paid to the effect of the perforated plate on the evolution of dynamical behavior downstream. The predicted results show an acceptable agreement with the experimental data. More specifically, the present work has led to the following main conclusions:

- The flow passing through the grid is divided into multiple jets. The jets adjacent to the tube wall undergo a pronounced deflection towards the tube core.
- A developing zone is observed downstream of the grid, a characteristic of the merging of the jets. A nearly uniform velocity distribution is attained at the streamwise position z/M=8.
- A rapid increase in the turbulent kinetic energy is observed between the positions z/M=0.5 and z/M=4.57 followed by a decay that is very rapid at first but becoming much slower further downstream.
- The turbulence is highly non-homogeneous in the near field with high intensities in high-shear regions.
- A nearly isotropic turbulence zone is noted at a streamwise position z/M=7.5, spreading over a streamwise distance of 2 M.

REFERENCES

[1] Zhou, L., Gao, D., Zhao, J., Wei, H., Zhang, X., Xu, Z., Chen, R. (2018). Turbulent flame propagation with pressure oscillation in the end gas region of confined combustion chamber equipped with different perforated plates. Combustion and Flame, 191: 453-467. https://doi.org/10.1016/j.combustflame.2018.01.023

[2] Boulahlib, M.S., Boukhalfa, M.A. (2016). Experimental study of premixed flame methane-air using a fine wire compensed thermometry. Journal of Applied Fluid Mechanics, 9(s2): 177-188. https://doi.org/10.36884/jafm.9.SI2.25770

[3] Goh, K.H.H., Geipel, P., Lindstedt, R.P. (2014). Lean premixed opposed jet flames in fractal grid generated multiscale turbulence. Combustion and Flame, 16: 2419-2434. https://doi.org/10.1016/j.combustflame.2014.03.010

[4] Sponfeldner, T., Soulopoulos, N., Beyrau, F., Hardalupas, Y., Taylor, A.M.K.P., Vassilicos, J.C. (2015). The structure of turbulent flames in fractal and regular grid generated turbulence. Combustion and Flame, 162: 3379-3393. https://doi.org/10.1016/j.combustflame.2015.06.004

[5] Coppola, G., Gomez, A. (2009). Experimental investigation on a turbulence generation system with high-blockage plates. Experimental Thermal and Fluid Science, 33: 1037-1048. https://doi.org/10.1016/j.expthermflusci.2009.06.001

[6] Buschmann, A., Dinkelacker, F., Schäfer, T., Schäfer, M., Wolfrum, J. (1996). Measurement of the instantaneous detailed flame structure in turbulent premixed combustion. Symposium (International) on Combustion, 26: 437-445. https://doi.org/10.1016/S0082-0784(96)80246-3

[7] Gagnepain, L. (1998). Contribution à l'étude de la structure des flammes turbulentes prémélangées pauvres : détermination des échelles caractéristiques des champs dynamique et scalaire. Doctoral thesis. Orléans. Université d'Orléans. Réf : 1998ORLE2041 – 87.

[8] Gagnepain, L., Chauveau, C., Gökalp, I. (1998). A comparison between dynamic and scalar timescales in lean premixed turbulent flames. Symposium (International) on Combustion, 27: 775-787. https://doi.org/10.1016/S0082-0784(98)80472-4

[9] Kalt, P.A.M., Frank, J.H., Bilger, R.W. (1998). Laser imaging of conditional velocities in premixed propane-air flames by simultaneous OH PLIF and PIV. Symposium (International) on Combustion, 27: 751-758. https://doi.org/10.1016/S0082-0784(98)80469-4

[10] Skiba, A.W., Wabel, T.M., Carter, C.D., Hammack, S.D., Temme, J.E., Driscoll, J.F. (2018). Premixed flames subjected to extreme levels of turbulence part I: flame structure and a new measured regime diagram. Combustion and Flame, 189: 407-432. https://doi.org/10.1016/j.combustflame.2017.08.016

[11] Rodrigues, N.S., Busari, O., Senior, W.C., McDonald, C.T., North, A.J., Chen, Y., Laster, W.R., Meyer, S.E., Lucht, R.P. (2019). The development and performance of a perforated plate burner to produce vitiated flow with negligible swirl under engine-relevant gas turbine conditions, Review of Scientific Instruments, 90: 075107. https://doi.org/10.1063/1.5100180

[12] Makita, H. (1991). Realization of a large-scale turbulence field in a small wind tunnel. Fluid Dynamics Research, 8: 53-64. https://doi.org/10.1016/0169-5983(91)90030-M

[13] Horender, S. (2013). Turbulent flow downstream of a large solidity perforated plate: Near-field characteristics of interacting jets. Fluid Dynamics Research, 45: 025501. https://doi.org/10.1088/0169-5983/45/2/025501

[14] Mazellier, N., Danaila, L., Renou, B. (2010). Multi-scale energy injection: A new tool to generate intense homogeneous and isotropic turbulence for premixed combustion. Journal of Turbulence, 11: 1-30. https://doi.org/10.1080/14685248.2010.519708

[15] Valente, P.C., Vassilicos, J.C. (2011). The decay of turbulence generated by a class of multiscale grids. Journal of Fluid Mechanics, 687: 300-340. https://doi.org/10.1017/jfm.2011.353

[16] Krogstad, P.A., Davidson, P.A. (2011). Freely decaying, homogeneous turbulence generated by multi-scale grids. Journal of Fluid Mechanics, 680: 417-434. https://doi.org/10.1017/jfm.2011.169

[17] Laizet, S., Vassilicos, J.C. (2011). DNS of fractal-generated turbulence. Flow Turbulence Combustion, 87: 673-705. https://doi.org/10.1007/s10494-011-9351-2

[18] Verbeek, A.A., Willems, P.A., Stoffels, G.G.M., Geurts, B.J., van der Meer, T.H. (2016). Enhancement of turbulent flame speed of V-shaped flames in fractal-grid-generated turbulence. Combustion and Flame, 167: 97-112. https://doi.org/10.1016/j.combustflame.2016.02.022
[19] Hurst, D., Vassilicos, J. (2007). Scaling and decay of fractal-generated turbulence. Physics of Fluids, 19: 035103. http://dx.doi.org/10.1063/1.2676448
[20] Soulopoulos, N., Kerl, J., Sponfeldner, T., Beyrau, F., Hardalupas, Y., Taylor, A.M.K.P., Vassilicos, J.C. (2013). Turbulent premixed flames on fractal-grid-generated turbulence. Fluid Dynamics Research, 45: 061404. https://doi.org/10.1088/0169-5983/45/6/061404
[21] Fragner, R., Mazellier, N., Halter, F., Chauveau, C., Gökalp, I. (2013). Multi-scale high intensity turbulence generator applied to a high pressure turbulent burner. Flow Turbulence Combustion, 94: 263-283. https://doi.org/10.1007/s10494-014-9556-2
[22] Wang, J., Yu, Q., Zhang, W., Zhang, M., Huang, Z., (2019). Development of a turbulence scale controllable burner and turbulent flame structure analysis. Experimental Thermal and Fluid Science, 109: 109898. https://doi.org/10.1016/j.expthermflusci.2019.109898
[23] Tanaka, E. (1970). The interference of two-dimensional parallel jets. 1st report, experiments on dual jet. Bulletin of JSME, 13: 272-280 https://doi.org/10.1299/jsme1958.13.272
[24] Comte-Bellot, G., Corrsin, S. (1966). The use of a contraction to improve the isotropy of grid-generated turbulence. Journal of Fluid Mechanics, 25: 657-682. https://doi.org/10.1017/S0022112066000338
[25] Hunt, J.C.R., Wray, A.A., Moin, P. (1988). Eddies, streams, and convergence zones in turbulent flows. Center for Turbulence Research Report CTR-S88, 193-208.

NOMENCLATURE

D	tube diameter, mm
d	grid hole diameter, mm
k	turbulent kinetic energy, m^2/s^2
L	tube length, mm
M	mesh size, mm
S	strain rate, 1/s
U_o	mean inlet velocity, m/s
U_x, U_y and U_z	mean velocity components in x, y and z directions respectively, m/s
u_x, u_y and u_z	root mean square (rms) velocity fluctuation components in x, y and z directions respectively, m/s

Greek symbols

ω	vorticity magnitude, 1/s
σ	blockage ratio